ELSEVIER

Materials Science and Engineering B 143 (2007) 14–20

MATERIALS SCIENCE & ENGINEERING B

www.elsevier.com/locate/mseb

Structure and lithium ion conductivity of bismuth containing lithium garnets $Li_5La_3Bi_2O_{12}$ and $Li_6SrLa_2Bi_2O_{12}$

Ramaswamy Murugan [a,*], Werner Weppner [a,*], Peter Schmid-Beurmann [b], Venkataraman Thangadurai [c]

[a] *Sensors and Solid State Ionics, Faculty of Engineering, University of Kiel, Kaiserstr. 2, D24143-Kiel, Germany*
[b] *Mineralogisches Institut der Westf. Wilhelms Universität Münster, Corrensstr. 24, 48149-Münster, Germany*
[c] *Department of Chemistry, University of Calgary, 2500 University Drive NW, Calgary, Alta. T2N 1N4, Canada*

Received 25 April 2007; received in revised form 2 July 2007; accepted 7 July 2007

Abstract

We report the synthesis, structure and transport properties of the new chemical compositions $Li_5La_3Bi_2O_{12}$ and $Li_6SrLa_2Bi_2O_{12}$. Qualitative phase analysis by X-ray powder diffraction patterns in combination with the Rietveld method revealed garnet type compounds as major phases. Whereas $Li_5La_3Bi_2O_{12}$ was found to be a single-phase material, $BiLa_2O_{4.5}$ could be identified as an impurity phase in the case of $Li_6SrLa_2Bi_2O_{12}$. Lithium ion conductivities of $Li_5La_3Bi_2O_{12}$ and $Li_6SrLa_2Bi_2O_{12}$ were studied by ac impedance method. The grain-boundary contribution to the total (bulk + grain-boundary) resistance is appreciable and amounts to about 54% and 61% for $Li_5La_3Bi_2O_{12}$ and $Li_6SrLa_2Bi_2O_{12}$, respectively, at 22 °C. $Li_6SrLa_2Bi_2O_{12}$ exhibits the highest total (bulk + grain-boundary) and bulk ionic conductivity of 2.0×10^{-5} and 5.2×10^{-5} S/cm, respectively, at 22 °C. The bismuth containing lithium garnet exhibits a maximum cubic lattice constant and the best lithium ion conductivity with low activation energy in the $Li_5La_3M_2O_{12}$ (M = Ta, Nb, Sb and Bi) series.

Keywords: Garnet-like structure; Solid-electrolyte; Li ion conductivity; ac conductivity; Lithium ion batteries

1. Introduction

There is presently a strong ongoing search for materials for energy conversion and storage. Fast lithium ion conducting solid electrolytes have drawn much attention due to their potential application in all-solid-state rechargeable (secondary) batteries and also in other solid-state electrochemical devices [1–5]. Lithium ion conduction has been reported for a wide range of crystalline metal oxides and halides with different types of structure [1–5]. Some oxides are excellent lithium ion conductors, e.g., $Li_{3x}La_{(2/3)-x}\square_{(1/3)-2x}TiO_3$ $(0 < x < 0.16)$ (LLT, where $\square$ represents a vacancy), which exhibits a bulk conductivity of 10^{-3} S/cm at 27 °C and $x \sim 0.1$ [6–8]. Since polycrystalline materials are being used for practical applications, large grain-boundary resistances are commonly observed in addition to the bulk resistance and therefore control the total (bulk + grain-boundary) resistance of the galvanic cells. For instance, $Li_{3x}La_{(2/3)-x}\square_{(1/3)-2x}TiO_3$ $(0 < x < 0.16)$ (LLT, where $\square$ represents a vacancy) exhibits a bulk conductivity of 10^{-3} S/cm and a total (bulk + grain-boundary) conductivity of 7×10^{-5} S/cm at 27 °C and $x \sim 0.1$ [6–8].

Recently, a novel class of fast lithium ion conducting metal oxides with the nominal chemical composition $Li_5La_3M_2O_{12}$ (M = Nb, Ta) possessing garnet-related structure has been reported from our laboratory [9,10]. Based on these compounds, further investigations of conductivity optimization by chemical substitutions and structural modifications were initiated. The partial replacement of divalent alkaline earth ions for a trivalent La in $Li_5La_3M_2O_{12}$ (M = Nb, Ta) extended the series of garnet-like structures by compounds with the general chemical formulas $Li_6ALa_2Nb_2O_{12}$ (A = Ca, Sr, Ba) [11] and $Li_6ALa_2Ta_2O_{12}$ (A = Sr, Ba) [12,13]. Also, partial substitution of trivalent La by monovalent K and pentavalent Nb by trivalent In in $Li_5La_3Nb_2O_{12}$ yielded new members of garnet-like materials [14]. Recently we investigated the structure and transport properties of $Li_5La_3Sb_2O_{12}$ and $Li_6SrLa_2Sb_2O_{12}$ [15].

* Corresponding authors.
E-mail addresses: rm@tf.uni-kiel.de (R. Murugan), ww@tf.uni-kiel.de (W. Weppner), psb@uni-muenster.de (P. Schmid-Beurmann), vthangad@ucalgary.ca (V. Thangadurai).

0921-5107/$ – see front matter © 2007 Elsevier B.V. All rights reserved.
doi:10.1016/j.mseb.2007.07.009

For further understanding the composition–structure–electrical conductivity relationships in the lithium containing garnet-related materials, further investigations were initiated to isolate new phases. Herein, we report for the first time the synthesis, structure and transport properties of the new chemical compositions $Li_5La_3Bi_2O_{12}$ and $Li_6SrLa_2Bi_2O_{12}$ with garnet-related structure.

2. Experimental

Conventional solid-state reaction procedure was employed to prepare the title compounds. Appropriate amounts of high purity chemicals $LiNO_3$ (Sigma–Aldrich, >99%, 10 wt% excess was added to compensate for the loss of lithium during annealing), $Sr(NO_3)_2$ (Riedel-deHaen, >99%), La_2O_3 (Alfa Aesar, >99.99%, pre-dried at 900 °C for 24 h) and Bi_2O_3 (Strem chemicals, USA, >99.9%) were ball-milled using zirconia balls in 2-propanol for about 12 h. After the evaporation of solvents at room temperature, the mixtures were heated to 675 °C in air, kept for 12 h at this temperature and then cooled down to room temperature. The resulting powders were ground again for another 12 h using zirconia balls in 2-propanol. After the evaporation of solvents, the powders were pressed into pellets by isostatic pressure and annealed at 750 °C in air for 6 h. The pellets were crushed into fine powder and again pressed into pellets by isostatic pressure and annealed at 775 °C for $Li_5La_3Bi_2O_{12}$ and 750 °C for $Li_6SrLa_2Bi_2O_{12}$ in air for 48 h while the samples were covered with powder of the same mother compound.

Sintered pellets of the furnace cooled samples were cut into small coin shaped cylinders. A portion of the pellet was ground to fine powder for phase characterisation. X-ray powder patterns were recorded using a powder diffractometer (SIEMENS D5000) with Cu Kα radiation and a secondary graphite (0 0 1) monochromator with the operation conditions $U = 40$ kV and $I = 30$ mA.

Qualitative phase analysis of the samples was made using the EVA-package of DiffracPlus software (BRUKER, Germany). Rietveld refinement was performed using the FULLPROF SUITE 2000 [16] program on the basis of Pseudo-Voigt profile functions. The starting parameters for the Li-(Sr,La)-Bi garnet phases were adopted from Cussen et al. [17]. Li atomic coordinates and occupancies were kept constant due to too low scattering power of Li in X-ray powder diffraction. Structural data for $BiLa_2O_{4.5}$ were taken from Wolcyrz et al. [18] into account.

Electrical conductivity measurements of the prepared pellets ($Li_5La_3Bi_2O_{12}$: 0.22 cm in thickness and 1.17 cm in diameter for thin pellet and 0.94 cm in thickness and 1.06 cm in diameter for thick pellet; $Li_6SrLa_2Bi_2O_{12}$: 0.28 cm in thickness and 1.17 cm in diameter for thin pellet and 1.04 cm in thickness and 1.07 cm in diameter for thick pellet) were performed in argon flow using Li-ion blocking Au-electrodes (Au paste cured at 700 °C for 1 h) in the temperature range from 24 to 300 °C using an impedance and gain-phase analyzer (HP 4192 A, Hewlett–Packard Co., Palo Alto, CA) (5 Hz–13 MHz). Prior to each impedance measurement, the samples were equilibrated for 3–6 h at constant temperature. For each sample, the impedance measurements were made for two heating and cooling cycles consecutively.

The microstructures of the sintered pellets were observed by means of a scanning electron microscope (SEM) (PHILIPS XL 30 Series, The Netherlands).

Table 1
Qualitative phase analysis and lattice parameters from pattern matching for $Li_5La_3Bi_2O_{12}$ and $Li_6SrLa_2Bi_2O_{12}$ garnets at room temperature

Composition	Phases detected	Lattice parameter
$Li_5La_3Bi_2O_{12}$	Garnet type $Li_5La_3Bi_2O_{12}$	1.30652(4) nm
$Li_6SrLa_2Bi_2O_{12}$	Garnet type $Li_6SrLa_2Bi_2O_{12}$, $BiLa_2O_{4.5}$ PDF 47-298 [29]	1.30893(9) nm, $a = 0.6829(2)$ nm, $b = 0.3997(1)$ nm $c = 0.4056(1)$ nm, $\beta = 125.11(2)^\circ$

3. Results and Discussion

The results of the qualitative and quantitative phase analysis on the basis of X-ray powder diffractions are given in Table 1.

According to our qualitative phase analysis, the synthesis route in the case of $Li_5La_3Bi_2O_{12}$ resulted in a phase pure garnet type compound (Fig. 1). In contrast to that, in case of the powder diffraction pattern of $Li_6SrLa_2Bi_2O_{12}$ the compound $BiLa_2O_{4.5}$ could be identified besides the major garnet type phase. As can be seen from Fig. 2 in the 2ϑ-range between 21 and 26° there is a number of weak reflections near the detection limit of the method which could not be attributed to any of these phases, e.g. by an indexing using the cubic lattice parameters of the garnet phases.

According to Cussen [17,19], the description of the structure of Li-garnets of the type $Li_5La_3M_2O_{12}$ (M = Nb, Ta, Sb) in the space group $Ia\bar{3}d$ is superior to a description in the space groups $I2_1a$ or $Ia\bar{3}$. The latter space groups of lower symmetry were applied formerly by other authors [20–23]. Since the powder diffractions of the mentioned Li-garnets did not show any Bragg peaks which violate the rules of the higher symmetry space group $Ia\bar{3}d$, this one is preferred for the structural description of these phases. Recently we have shown [15] that the structural model

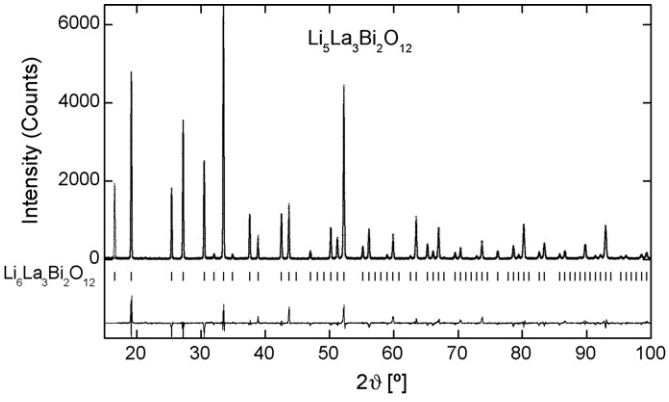

Fig. 1. Observed (dots), calculated (line), allowed Bragg peak positions for the garnet phase (upper markers) and difference X-ray powder diffraction pattern (lower marker) collected from $Li_5La_3Bi_2O_{12}$ at room temperature.

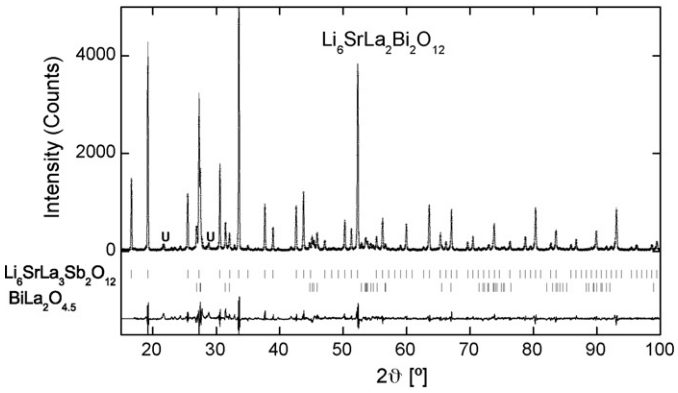

Fig. 2. Observed (dots), calculated (line), allowed Bragg peak positions for the garnet phase (upper markers) and $BiLa_2O_{4.5}$ (intermediate markers) and difference X-ray powder diffraction pattern (lower marker) collected from $Li_6SrLa_2Bi_2O_{12}$ at room temperature.

of Cussen et al. [17] can be also successfully applied to the structures of Li–Sb-garnets of the type $Li_{5+n}Sr_nLa_{3-n}Sb_2O_{12}$ ($n = 0$ and 1) [15]. The same hold here since the appearing Bragg peaks in the powder diffraction patterns of $Li_5La_3Bi_2O_{12}$ and $Li_6SrLa_2Bi_2O_{12}$ are in agreement with the reflections rules of space group $Ia\bar{3}d$ we used the structural data of Cussen et al. [17] in order to fit our powder diffractions. The results are given in Figs. 1 and 2 as well as in Tables 1 and 2.

According to Table 1, the coupled substitution $La^{3+} \Leftrightarrow Sr^{2+} + Li^+$ is correlated with an increase in the lattice parameter a. This effect was already observed for Li-garnets of the type $Li_{5+n}Sr_nLa_{1-n}Sb_2O_{12}$ ($n = 0$, 1) [15]. The cubic lattice constant increases by substitution of divalent Sr for a trivalent La in $Li_5La_3Bi_2O_{12}$, which corresponds to the increasing ionic size of the eight-coordinated Sr^{2+} (0.125 nm) compared to the corresponding value for La^{3+} (0.118 nm) [24].

Table 2
Structural parameters of Li–(La,Sr)–(Bi)–O garnets from Rietveld refinement of X-ray powder diffractions at room temperature (space group $Ia\bar{3}d$)

	Site	$Li_5La_3Sb_2O_{12}$ [17]	$Li_5La_3Bi_2O_{12}$	$Li_6SrLa_2Bi_2O_{12}$
(Bi, Sb) x, y, z	24c	1/8, 0, 1/4	1/8, 0, 1/4	1/8, 0, 1/4
(La, Sr) x, y, z	16a	0, 0, 0	0, 0, 0	0, 0, 0
Li1-t x, y, z	24d	1/4, 7/8, 0	1/4, 7/8, 0	1/4, 7/8, 0
Occupancy		*0.793(8)*	*0.793*	*0.793*
Li2-oc x	96h	*0.107(1*	*0.107*	*0.107*
y		*0.6676(8)*	*0.6676*	*0.6676*
z		*0.6171(8)*	*0.6171*	*0.617*
Occupancy		*0.218(2)*	*0.218*	*0.218* + 0.0833*
O x	96h	*0.27994(4)*	0.282(2)	0.281(3)
y		*0.10666(5)*	0.097(3)	0.101(3)
z		*0.19932(5)*	0.189(2)	0.194(3)
a [nm]		*1.28518(3)*	1.30652(4)	1.30893(9)
$B_{overall}$			0.38(5)	0.27(5)
R_p/R_{wp}			12.0/14.7	13.4/18.5
GOF/R_{exp}			1.7/7.9	2.1/8.9
R_{Bragg}			9.9	4.7

Note: Data in italics are taken from Cussen [17]. Site occupancies for oxygen were set to unity. *In order to model the Li-distribution in $Li_6SrLa_2Bi_2O_{12}$ it was assumed that the additional Li enters completely the Li (96h) position.

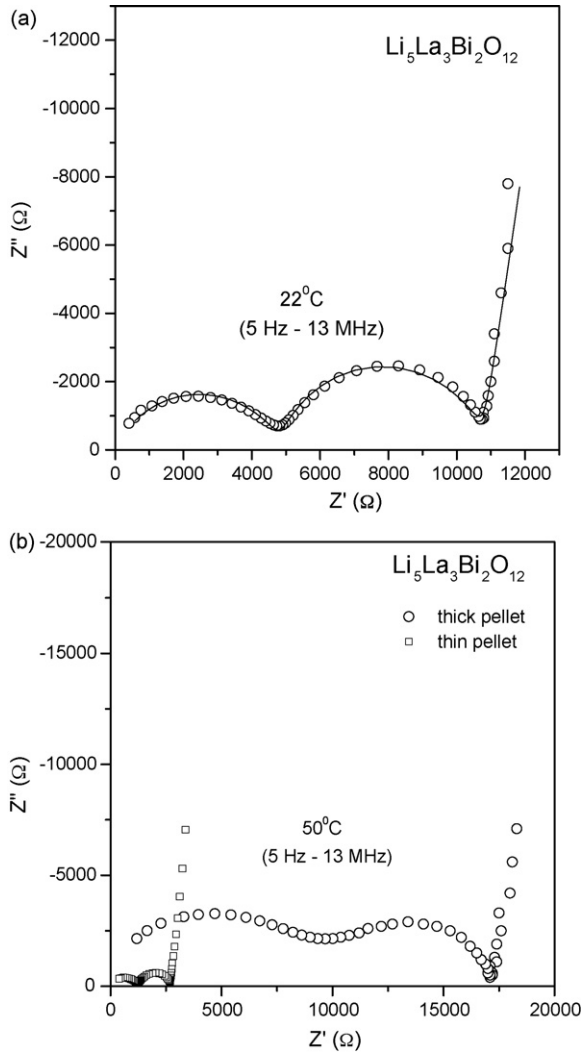

Fig. 3. ac impedance plot of $Li_5La_3Bi_2O_{12}$: (a) thin pellet at 22 °C and (b) thin and thick pellet at 50 °C. The solid line represents simulated data with an equivalent circuit consisting of $(R_bQ_b)(R_{gb}Q_{gb})(Q_{el.})$ (where R is the resistance and Q is the constant phase element and the subscripts g, gb and el refer to the grain, grain-boundary and electrode, respectively) using the EQUIVALENT program [28].

A typical impedance plot obtained at 22 °C for a thin pellet of $Li_5La_3Bi_2O_{12}$ is shown in Fig. 3a. For comparison, the impedance plots obtained at 50 °C for both the thick and thin pellets of $Li_5La_3Bi_2O_{12}$ are shown in Fig. 3b. Impedance plot obtained at 22 °C for the thin pellet and at 50 °C for both the thick and thin pellet of $Li_6SrLa_2Bi_2O_{12}$ are shown in Fig. 4a and b, respectively. The appearance of a capacitive tail at the low frequency side in the case of the applied ionically blocking electrodes is an indication that the investigated material is ionically conducting in nature [25–27]. A similar behaviour has been observed for the earlier investigated materials with garnet-related structure [9,11–14]. The impedance plot could be well resolved into bulk, grain-boundary and electrode resistances. The solid line in Figs. 3a and 4a represents fitted data with an equivalent circuit consisting of $(R_bQ_b)(R_{gb}Q_{gb})(Q_{el})$ using the EQUIVALENT program [28]. The bulk and grain-boundary resistance, constant phase angle element of bulk and

Table 3
Impedance data for thin pellets of $Li_5La_3Bi_2O_{12}$ and $Li_6SrLa_2Bi_2O_{12}$ at 22 °C in argon

Compound	R_b† (Ω)	Q_b† (F)	R_{gb}† (Ω)	Q_{gb}† (F)	σ_{bulk}† (S cm^{-1})	σ_{total}† (S cm^{-1})	$R_{gb}/(R_b+R_{gb})$
$Li_5La_3Bi_2O_{12}$	4865	1.10×10^{-9}	5875	5.56×10^{-8}	4.0×10^{-5}	1.9×10^{-5}	0.54
$Li_6SrLa_2Bi_2O_{12}$	4990	1.17×10^{-9}	7810	6.21×10^{-8}	5.2×10^{-5}	2.0×10^{-5}	0.61

† Where R is the resistance and Q is the constant phase element and the subscripts b and gb refer to the bulk and grain boundary, respectively. σ_{bulk} and σ_{total} represents bulk conductivity and total (bulk + grain-boundary) conductivity, respectively.

grain-boundary, bulk and total (bulk + grain-boundary) conductivity and the ratio between the grain-boundary resistance and total (bulk + grain-boundary) resistance obtained at 22 °C for thin pellets of $Li_5La_3Bi_2O_{12}$ and $Li_6SrLa_2Bi_2O_{12}$ are tabulated in Table 3. The grain-boundary contribution to the total (bulk + grain-boundary) resistance is appreciable and amounts to about 54% and 61% for $Li_5La_3Bi_2O_{12}$ and $Li_6SrLa_2Bi_2O_{12}$, respectively, at 22 °C.

Previously, we have observed that the alkaline earth ion substitution for La and simultaneous addition of Li for charge compensation in the parent compound $Li_5La_3M_2O_{12}$ (M = Nb, Ta) [11–13] reduces the grain-boundary contribution. In the present work, the strontium substituted $Li_6SrLa_2Bi_2O_{12}$ exhibits a slight increase in the grain-boundary contribution to the total resistance compared to $Li_5La_3Bi_2O_{12}$. The impedance measurements were carried out for two different dimensions in order to find out whether the second semi-circle appearing

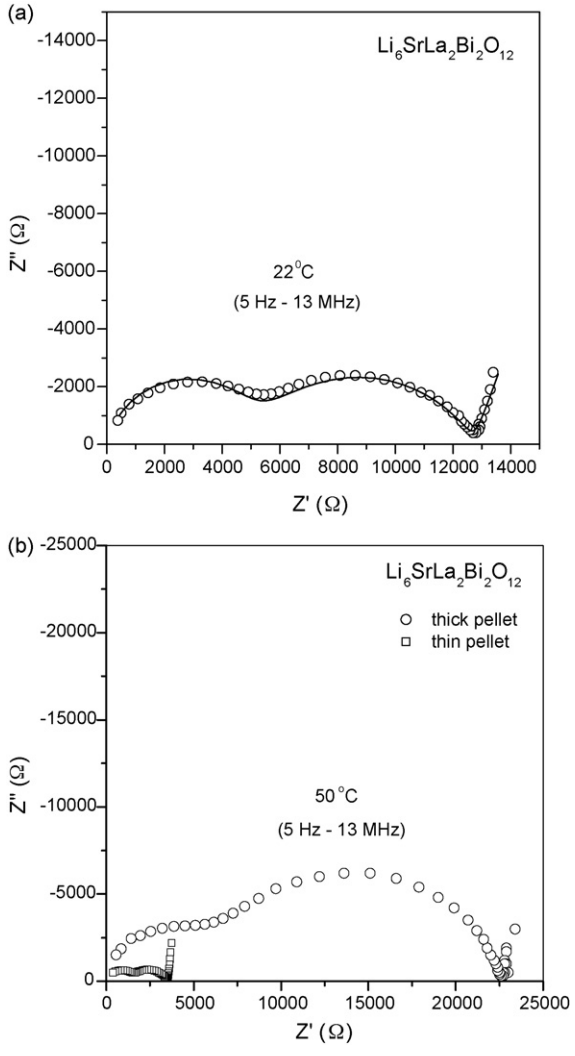

Fig. 4. ac impedance plot of $Li_6SrLa_2Bi_2O_{12}$: (a) thin pellet at 22 °C and (b) thin and thick pellet at 50 °C. The solid line represents simulated data with an equivalent circuit consisting of $(R_bQ_b)(R_{gb}Q_{gb})(Q_{el.})$ (where R is the resistance and Q is the constant phase element and the subscripts g, gb and el refer to the grain, grain-boundary and electrode, respectively) using the EQUIVALENT program [28].

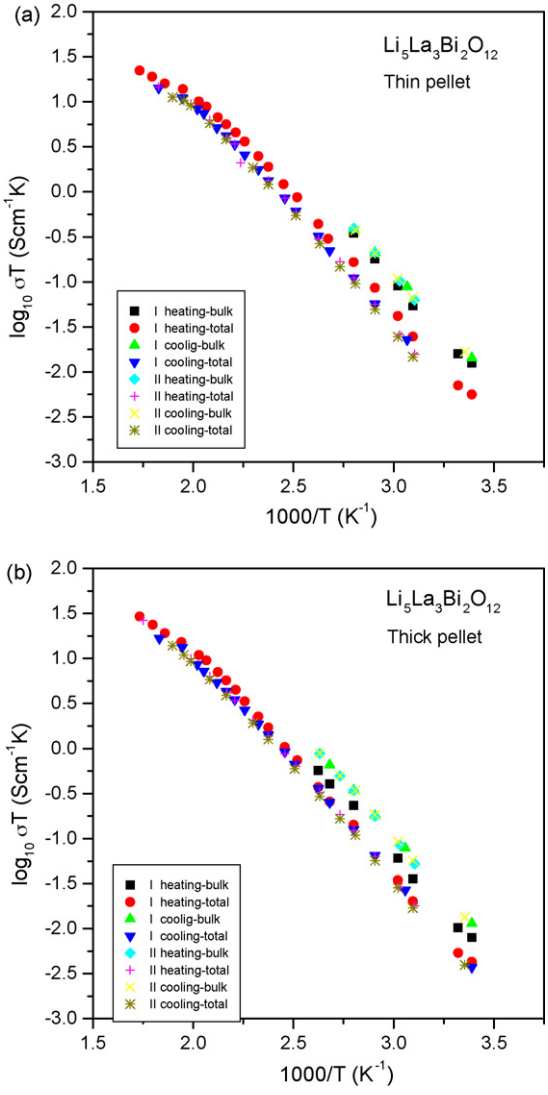

Fig. 5. Arrhenius plots of $Li_5La_3Bi_2O_{12}$ for (a) total (bulk + grain-boundary) and bulk lithium ion conductivity of thin pellet and (b) total (bulk + grain-boundary) and bulk lithium ion conductivity of thick pellet. The data were obtained from two heating and cooling cycles consecutively in argon.

at low-frequency is due to grain-boundary phenomena or due to the surface electrodes. The impedance plots presented in Figs. 3b and 4b clearly indicate a similar behavior exhibited by both the thin and thick pellets of the compounds and indicates that the second semi-circle in the low-frequency regime is related to the grain-boundary phenomena.

The bulk (5.2×10^{-5} S cm^{-1}) and total conductivity (2.0×10^{-5} S cm^{-1}) of $Li_6SrLa_2Bi_2O_{12}$ are slightly higher than the bulk (4.0×10^{-5} S cm^{-1}) and total conductivity (1.9×10^{-5} S cm^{-1}) obtained for $Li_5La_3Bi_2O_{12}$ at 22 °C (Table 3). The slight increase in the bulk as well as total conductivity with the substitution of strontium for lanthanum with simultaneous addition of lithium in $Li_5La_3Bi_2O_{12}$ is similar to the observation made for the Ta containing garnet $Li_5La_3Ta_2O_{12}$ [12]. At higher temperature (above 110 °C), it is difficult to separate bulk and grain-boundary contributions accurately; accordingly, we have considered the total (bulk + grain-boundary) contribution for the determination of electrical conductivity over the investigated temperature range.

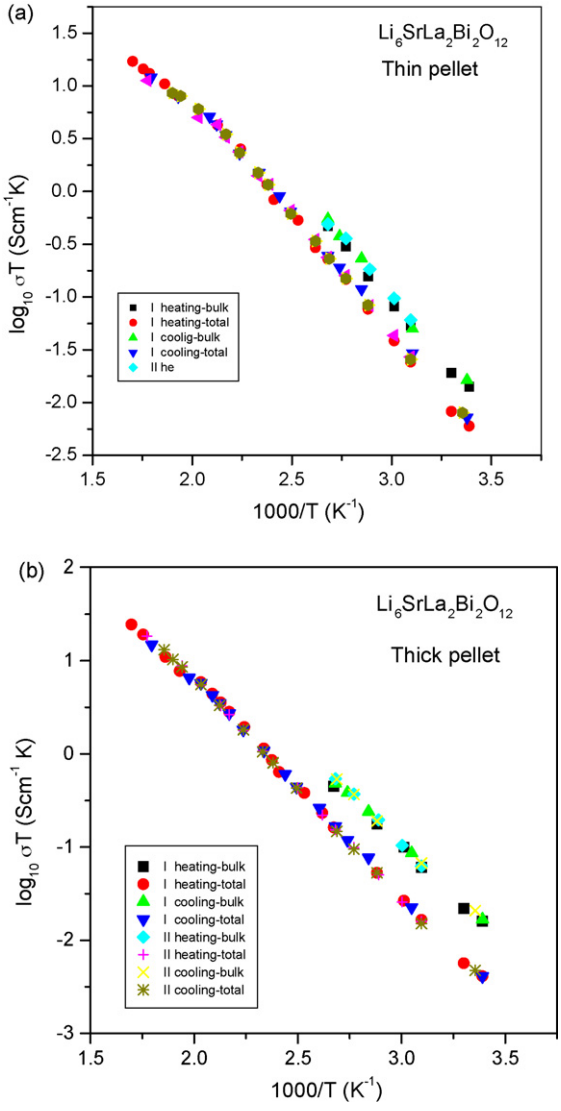

Fig. 6. Arrhenius plots of $Li_6SrLa_2Bi_2O_{12}$ for (a) total (bulk + grain-boundary) and bulk lithium ion conductivity of thin pellet and (b) total (bulk + grain-boundary) and bulk lithium ion conductivity of thick pellet. The data were obtained from two heating and cooling cycles consecutively in argon.

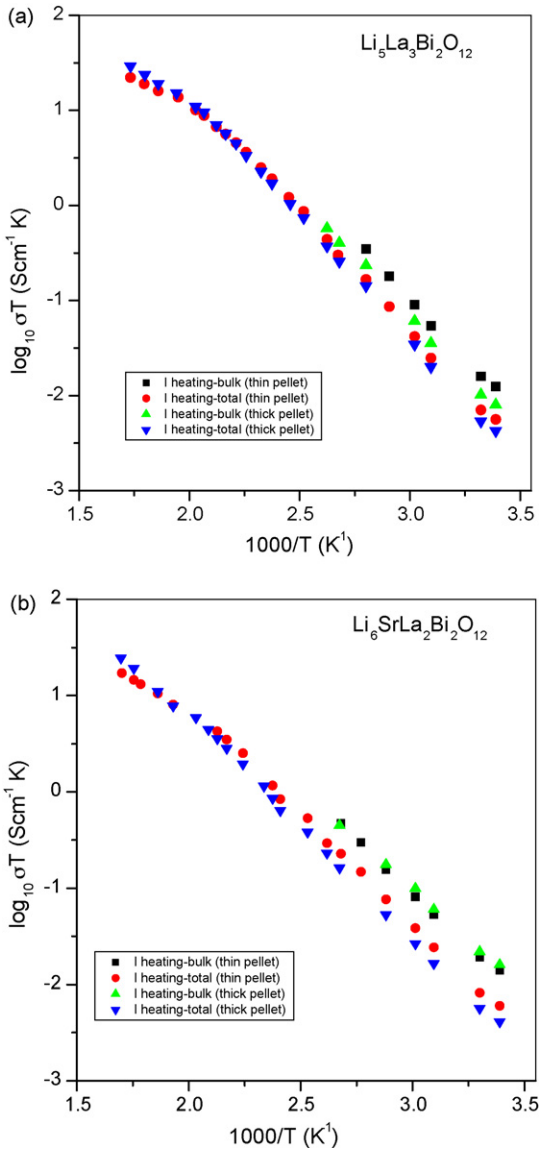

Fig. 7. Comparison of Arrhenius plots of total (bulk + grain-boundary) and bulk lithium ion conductivity of thin and thick pellets of (a) $Li_5La_3Bi_2O_{12}$ and (b) $Li_6SrLa_2Bi_2O_{12}$ during the first heating process.

The Arrhenius plots for the total (bulk + grain-boundary) and bulk electrical conductivity of thin and thick pellets of $Li_5La_3Bi_2O_{12}$ and $Li_6SrLa_2Bi_2O_{12}$ are shown in Figs. 5a and b and 6a and b, respectively. The data obtained from heating and cooling runs almost follow the same line, which implies that the investigated garnet-like structure compounds are thermally stable without any phase transition in the investigated temperature range between room temperature and 300 °C. For comparison, the Arrhenius representations for thin and thick pellets of $Li_5La_3Bi_2O_{12}$ and $Li_6SrLa_2Bi_2O_{12}$ obtained during the first heating process shown in Fig. 7a and b, respectively, indicate a similar electrical conductivity behavior exhibited by both thick and thin pellets.

The activation energies (E_a) for the ionic conductivity were determined from the Arrhenius plots employing the equation:

$$\sigma T = A \exp\left[-\frac{E_a}{kT}\right] \quad (1)$$

where A is the pre-exponential parameter, k is Boltzmann's constant and T is the absolute temperature.

The activation energies for the bulk lithium ion conductivity (from 22 to 100 °C) of the thin pellets of $Li_5La_3Bi_2O_{12}$ and $Li_6SrLa_2Bi_2O_{12}$ are 0.49 and 0.43 eV, respectively. The activation energies for the total (bulk + grain-boundary) lithium ion conductivity (from 22 to 300 °C) of thin pellets of $Li_5La_3Bi_2O_{12}$ and $Li_6SrLa_2Bi_2O_{12}$ are 0.47 and 0.42 eV, respectively. The activation energies obtained for the total (bulk + grain-boundary) lithium ion conductivity of $Li_5La_3Bi_2O_{12}$ and $Li_6SrLa_2Bi_2O_{12}$ are comparable to other garnet-related fast lithium ion conductors such as $Li_5La_3Ta_2O_{12}$ (0.56 eV) [9], $Li_5La_3Nb_2O_{12}$ (0.55 eV) [14], $Li_6CaLa_2Nb_2O_{12}$ (0.55 eV) [11], $Li_6SrLa_2Nb_2O_{12}$ (0.50 eV) [11], $Li_6BaLa_2Nb_2O_{12}$ (0.44 eV) [11], $Li_6SrLa_2Ta_2O_{12}$ (0.50 eV) [12], $Li_6BaLa_2Ta_2O_{12}$ (0.40 eV) [12], $Li_{5.5}La_3Nb_{1.75}In_{0.25}O_{12}$ (0.49 eV) [14] and $Li_{5.5}La_{2.75}K_{0.25}Nb_2O_{12}$ (0.53 eV) [14].

The grain-boundary contribution to the total (bulk + grain-boundary) resistance is appreciable for $Li_5La_3Bi_2O_{12}$ and $Li_6SrLa_2Bi_2O_{12}$ at 22 °C. Scanning electron microscope (SEM) images of the $Li_5La_3Bi_2O_{12}$ compound shown in Fig. 8a revealed poor sintering which leads to an appreciable grain-boundary contribution to the total resistance. The SEM image (Fig. 8b) of $Li_6SrLa_2Bi_2O_{12}$ also revealed poor sintering as well as the presence of second phases. Both the presence of second phases ($BiLa_2O_{4.5}$ and unidentified phase) and poor sintering appear to be the reason for the observed larger grain-boundary contribution to the total resistance in $Li_6SrLa_2Bi_2O_{12}$.

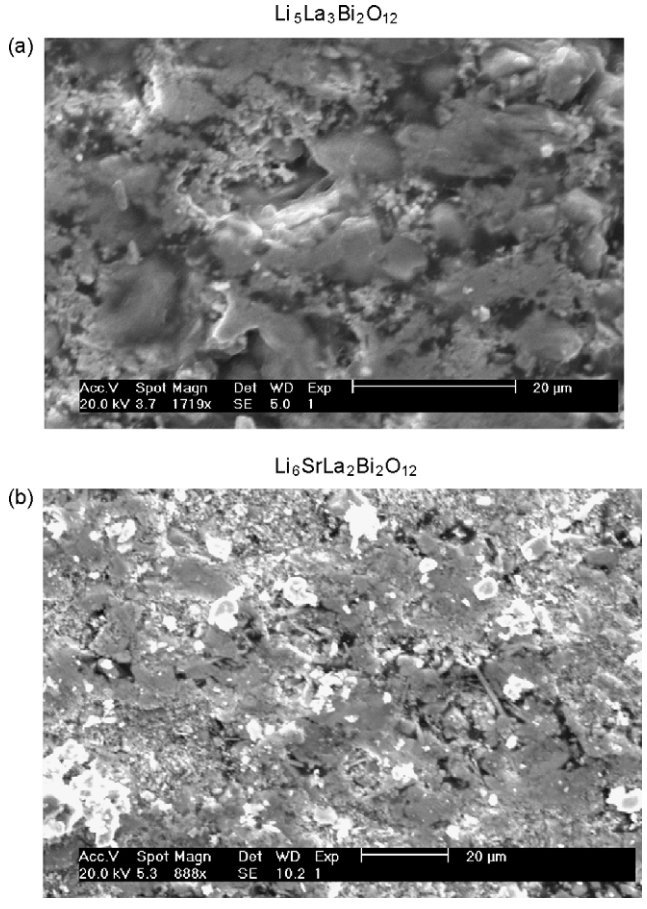

Fig. 8. SEM images of (a) $Li_5La_3Bi_2O_{12}$ and (b) $Li_6SrLa_2Bi_2O_{12}$.

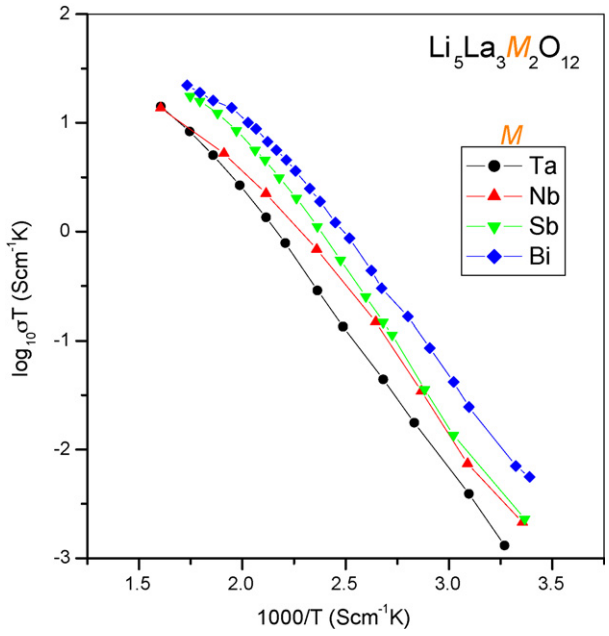

Fig. 9. Comparison of Arrhenius plots of total (bulk + grain-boundary) lithium ion conductivity of the $Li_5La_3M_2O_{12}$ (M = Ta [9], Nb [14], Sb [15] and Bi) series.

The Arrhenius representations of the total (bulk + grain-boundary) ionic conductivities of $Li_5La_3Ta_2O_{12}$ [9], $Li_5La_3Nb_2O_{12}$ [14], $Li_5La_3Sb_2O_{12}$ [15] and $Li_5La_3Bi_2O_{12}$ (the present work) are presented in Fig. 9 for comparison.

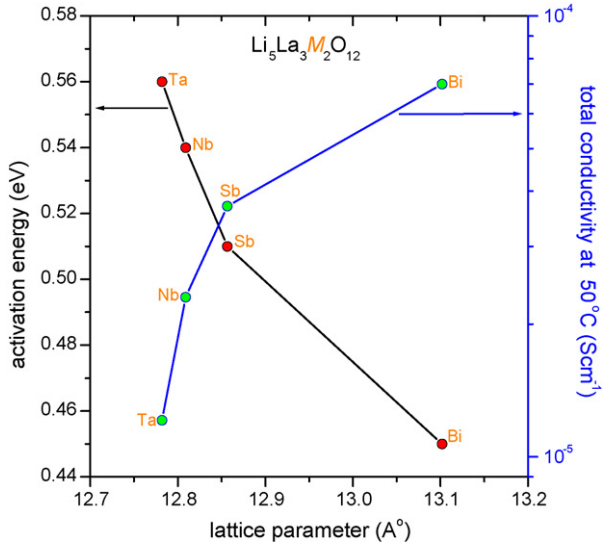

Fig. 10. Dependence of the total (bulk + grain-boundary) ionic conductivity and activation energy vs. lattice parameter of the $Li_5La_3M_2O_{12}$ (M = Ta [9], Nb [14], Sb [15] and Bi) series.

The dependence of the total (bulk + grain-boundary) ionic conductivity and activation energy versus lattice parameter of the $Li_5La_3M_2O_{12}$ (M = Ta [9], Nb [14], Sb [15] and Bi) series is shown in Fig. 10. It is interesting to note that the lattice parameter and ionic conductivity increases in the order Ta < Nb < Sb < Bi and the activation energy increases in the opposite order Ta > Nb > Sb > Bi in the $Li_5La_3M_2O_{12}$ (M = Ta [9], Nb [14], Sb [15] and Bi) series. The increase in conductivity with decreasing activation energy is accompanied by the lattice expansion for the investigated $Li_5La_3M_2O_{12}$ series which indicates that there is a systematic correlation between the lattice expansion with the increase in ionic conductivity.

4. Summary

New chemical compositions $Li_5La_3Bi_2O_{12}$ and $Li_6SrLa_2Bi_2O_{12}$ with garnet-like structure with predominant ionic conduction as members of the $Li_5La_3M_2O_{12}$ series were isolated for the first time. Ac impedance studies indicated that the grain-boundary contribution to the total (bulk + grain-boundary) resistance is appreciable and about 54 and 61% for $Li_5La_3Bi_2O_{12}$ and $Li_6SrLa_2Bi_2O_{12}$, respectively, at 22 °C. $Li_6SrLa_2Bi_2O_{12}$ exhibits slightly better total (bulk + grain-boundary) as well as bulk ionic conductivity at room temperature. A systematic correlation between the lattice expansion with an increase in ionic conductivity was observed in $Li_5La_3M_2O_{12}$ (M = Ta, Nb, Sb and Bi) lithium garnets.

Acknowledgement

The authors would like to thank the German Science Foundation (DFG grant WE 684/11-1) for financial support.

References

[1] A.D. Robertson, A.R. West, A.G. Ritchie, Solid State Ionics 104 (1997) 1–11.
[2] (a) G.Y. Adachi, N. Imanaka, H. Aono, Adv. Mater. 8 (1996) 127–135; (b) T. Kudo, in: P.J. Gellings, H.J.M. Bouwmeester (Eds.), The CRC Handbook of Solid State Electrochemistry, CRC Press, London, 1997, p. 195.
[3] C. Julien, G.A. Nazri, Solid State Batteries: Materials Design and Optimization, Kluwer Academic Publications, Boston, 1994.
[4] H. Aono, N. Imanaka, G.Y. Adachi, Acc. Chem. Res. 27 (1991) 265–270.
[5] J.T.S. Irvine, A.R. West, in: T. Takahashi (Ed.), High Conductivity Solid Ionic Conductors, Recent Trends and Applications, World Scientific, Singapore, 1989, p. 201.
[6] Y. Inaguma, C. Liquan, M. Itoh, T. Nakamura, T. Uchida, H. Ikuta, W. Wakihara, Solid State Commun. 86 (1993) 689–693.
[7] H. Kawai, J. Kuwano, J. Electrochem. Soc. 141 (1994) L78–L79.
[8] O. Bohnke, C. Bohnke, J.L. Fourquet, Solid State Ionics 91 (1996) 21–31.
[9] V. Thangadurai, H. Kaack, W. Weppner, J. Am. Ceram. Soc. 86 (2003) 437–440.
[10] V. Thangadurai, S. Adams, W. Weppner, Chem. Mater. 16 (2004) 2998–3006.
[11] V. Thangadurai, W. Weppner, J. Am. Ceram. Soc. 88 (2005) 411–418.
[12] V. Thangadurai, W. Weppner, Adv. Funct. Mater. 15 (2005) 107–112.
[13] V. Thangadurai, W. Weppner, J. Power Sources 142 (2005) 339–344.
[14] V. Thangadurai, W. Weppner, J. Solid State Chem. 179 (2006) 974–984.
[15] R. Murugan, W. Weppner, P.S. Beurmann, V. Thangadurai, Mater. Res. Bull., submitted for publication.
[16] J. Rodriguez-Carvajal, Full Prof Suite, Lab. de Léon Brillouin (CEA-CNRS) CEA/Saclay, France, 2000.
[17] E.J. Cussen, Th.W.S. Yip, J. Solid State Chem. 180 (2007) 1832–1839.
[18] M. Wolcyrz, L. Kepinski, R. Horyn, J. Solid State Chem. 116 (1995) 72–76.
[19] E.J. Cussen, Chem. Commun. (2006) 412–413.
[20] D. Mazza, Mater. Lett. 7 (1988) 205–207.
[21] H. Hyooma, K. Hayashi, Mater. Res. Bull. 23 (1988) 1399–1407.
[22] J. Isasi, M.L. Veiga, R. Saez-Puche, A. Jereze, C. Pico, J. Alloys Compd. 177 (2) (1991) 251–257.
[23] J. Isasi, M.L. Veiga, A. Jereze, C. Pico, J. Less-Common Met. 167 (1991) 381–385.
[24] R.D. Shannon, Acta Crystallogr. A 32 (1976) 751–767.
[25] V. Thangadurai, R.A. Huggins, W. Weppner, J. Power Sources 108 (2002) 64–69.
[26] J.T.S. Irvine, D.C. Sinclair, A.R. West, Adv. Mater. 2 (1990) 132–138.
[27] J.E. Bauerle, J. Phys. Chem. Solids 30 (1969) 2657–2670.
[28] B.A. Boukamp, Equivalent Circuit, Version 4.55, 1997, Faculty of Chemical Technology, University of Twente, 7500 AE Enschede, The Netherlands, Reports No: CT88/265/128/CT89/214/128, 1989.
[29] X. Chen, W. Eysel, J. Solid State Chem. 124 (1996) 300–304.